https://doi.org/10.5194/egusphere-2025-3627
Preprint. Discussion started: 1 October 2025

Application and Evaluation of CRACMM V1.0 Mechanism in $PM_{2.5}$ Simulation Over China

Qingfang Su[1], Yifei Chen[1], Yangjun Wang[1*], David C. Wong[2,3], Havala O. T. Pye[2], Ling Huang[1], Golam Sarwar[2], Benjamin Murphy[2], Bryan Place[4], and Li Li[1*]

[1]Key Laboratory of Organic Compound Pollution Control Engineering (MOE), School of Environmental and Chemical Engineering, Shanghai University, Shanghai, 200444, China
[2]Office of Research and Development, U.S. Environmental Protection Agency, Research Triangle Park, North Carolina, USA
[3]Department of Earth and Atmospheric Sciences, University of Houston, Houston, USA
[4]Oak Ridge Institute for Science and Engineering (ORISE), Office of Research and Development, U.S. Environmental Protection Agency, Research Triangle Park, North Carolina, USA. Now at: SciGlob Instruments and Services, LLC., 9881 Broken Land Pkwy, Columbia, MD 21046, USA

Correspondence to: Li Li (lily@shu.edu.cn) and Yangjun Wang (yjwang326@shu.edu.cn)

Abstract

Chemical mechanisms are one of the major sources of bias in chemical transport model simulations, making their improvement a critical step towards enhancing model performance and supporting air quality management and research. In this study, a newly developed chemical mechanism, the Community Regional Atmospheric Chemistry Multiphase Mechanism (CRACMM), integrated into the Community Multiscale Air Quality (CMAQ) modeling system, was evaluated through comparison with two traditional chemical mechanisms, CB6r3_ae7 and Saprc07tic_ae7i, for China. Sensitivity simulations related to precursor reactive organic carbon (ROC) emissions were conducted to investigate the key driving factors of $PM_{2.5}$ formation. The results show slight differences in the correlation coefficient (R), mean bias (MB), and normalized mean bias (NMB) values for the three chemical mechanisms when using the traditional primary organic aerosol (POA) inventory. However, when using the full volatility emission inventory, CRACMM shows improvements in R, MB, and NMB values in some regions. CRACMM predicts higher $PM_{2.5}$ concentrations during spring, summer and autumn, mainly due to enhanced secondary organic aerosol (SOA) formation driven by increased precursor emissions. Benzene–toluene–xylene (BTX) species and semi-volatile organic compound (SVOC) emissions significantly contributed to $PM_{2.5}$ formation in CRACMM. The SOA from BTX emissions accounts for nearly 50% of the $PM_{2.5}$ changes, while intermediate-

https://doi.org/10.5194/egusphere-2025-3627
Preprint. Discussion started: 1 October 2025

volatility organic compounds (IVOC) and SVOCs emissions mainly affect $PM_{2.5}$ concentrations through SOA formation. These results indicate that CRACMM, when using the full volatile inventory, can effectively compensate for the underestimation of $PM_{2.5}$ mass that may occur with traditional POA treatment, particularly in regions with high photochemical activity and abundant S/IVOC precursors.

1. Introduction

Exposure to airborne $PM_{2.5}$ is associated with a variety of harmful health effects (2011; Liu et al., 2024; Kim et al., 2015) and was reported to cause 4.14 million deaths worldwide annually (95% confidence interval: 3.45 to 4.80) (Murray et al., 2020). Thus, a better understanding of the $PM_{2.5}$ formation mechanism is essential for formulating effective air pollution control strategies.

The Chemical Transport Models (CTMs) serve as valuable tools for identifying factors contributing to $PM_{2.5}$ formation. They can reproduce a series of physical and chemical processes that atmospheric pollutants undergo after being emitted into the atmosphere, driven by emission inventory data and meteorological fields. Gas-phase chemical reaction mechanisms are an essential part of the CTMs. Condensed mechanisms such as the Carbon-Bond (CB) mechanism (Yarwood et al., 2005; Yarwood et al., 2010) and the Statewide Air Pollution Research Center (SAPRC) mechanism (Carter, 2010, 1999; Carter, 2000) are widely used in CTMs. In these mechanisms, various volatile organic compounds (VOCs) are lumped into functional groups.

The CB chemical mechanism has evolved since the 1970s, with CB7 being one of the most recent versions. The carbon bonds are treated as a reaction unit, grouped by their bonding state, without explicitly marking their location within the molecule. Aerosol Module 7 (aero7) is the latest aerosol representation within the CMAQ model, developed by the U.S. Environmental Protection Agency (EPA). Aero7 improves consistency in representing SOA formation pathways between the CB- and SAPRC-based chemical mechanisms. It also updates monoterpene SOA yields from photooxidation, adds uptake of water onto hydrophilic organics, and includes consumption of inorganic sulfates (SO_4^{2-}) when isoprene epoxydiol (IEPOX) organosulfates are formed (Pye et al., 2013). Furthermore, it enhances computational efficiency by using a volatility basis set (VBS) to parameterize SOA yields rather than using the Odum 2-product fit (Zhang et al., 2021).

https://doi.org/10.5194/egusphere-2025-3627
Preprint. Discussion started: 1 October 2025

The SAPRC mechanism was first developed in the 1980s at the University of California, Riverside. Saprc07tic is one of the most widely used versions (Xie et al., 2013), which introduces refinements for isoprene chemistry. It is commonly used in regulatory and research applications requiring a detailed representation of VOCs. Saprc07tic is a detailed, explicit chemical mechanism that represents the atmospheric oxidation of a large number of VOCs, providing a more nuanced representation of ozone formation and SOA production. Aero7 and Aero7i modules contain the same major pathways to SOA, but AERO7i provides more diagnostic information in terms of IEPOX SOA identification (Pye et al., 2017; Pye et al., 2013), as well as some additional high-NO_x formation pathways to SOA (Pye et al., 2015).

CRACMM (Pye et al., 2023) is a state-of-the-art atmospheric chemistry mechanism and was introduced with the release of CMAQ version 5.4 in October 2022 by the U.S. EPA. CRACMM integrates gas-phase and particle-phase reactions, offering a wide-ranging representation of atmospheric processes and enhanced capabilities for simulating multiphase chemistry in regional air quality modeling. This approach helps models to more closely replicate photochemical processes that occur in the atmosphere. CRACMM builds upon the well-established Regional Atmospheric Chemistry Mechanism, version 2 (RACM2) framework (Goliff et al., 2013) and incorporates enhanced representations of various organic compounds, particularly monoterpenes and aromatics. Furthermore, CRACMM includes a built-in, transparent mapping of emissions to mechanism species, ensuring conservation of emitted carbon while tracking its transformation in products. CB6r3_ae7 and Saprc07tic_ae7i typically exclude organic species with saturation concentrations (C_i^*) in the low-volatility organic compound (LVOC, $0.3 < C_i^*$ μg m^{-3}), SVOC ($0.3 \leq C_i^* < 300$ μg m^{-3}) and IVOC ($300 \leq C_i^* < 3 \times 10^6$ μg m^{-3}) ranges, which act as potential precursors to SOA formation (Chang et al., 2022). SOA precursors beyond traditional, non-oxygenated volatile hydrocarbons such as S/IVOCs, phenolic compounds, furans, and other oxygenated organic compounds are considered in CRACMM (Pye et al., 2023).

Some previous studies have compared the model performance using various mechanisms in CTMs. Luecken et al. (2019) compared CB6r3, CB5TU, and CB5 performances, and found that CB6r3 performed best in simulating the vertical distribution of peroxyacyl nitrates. Derwent et al. (2017) found that the condensed mechanisms (including CB6r3) and Master

https://doi.org/10.5194/egusphere-2025-3627
Preprint. Discussion started: 1 October 2025

Chemical Mechanism version 3.3.1 (MCMv3.3.1) have large differences in predicted hydroxyl radical (HO·) concentrations and their responses to NO_x and VOC reductions. For the SAPRC mechanism, Kang et al., (2022) evaluated a highly condensed SAPRC chemical mechanism and found that Saprc07 predicts slightly lower O_3 concentrations than the standard fix-parameter version of the Saprc11. CRACMM predictions were compared with RACM2 and CB6r3 over the northeastern US during summer. The results showed that CRACMM tends to predict more O_3 than CB6r3 but less than RACM2 (Place et al., 2023). However, the $PM_{2.5}$ predictions by the newly developed CRACMM mechanism and their sensitivities to precursors have not yet been investigated. In this study, $PM_{2.5}$ predictions from the CRACMM mechanism were evaluated with surface observations comprehensively, covering different seasons and regions. Results derived by CRACMM are compared with two well-established chemical mechanisms, Saprc07tic_ae7i and CB6r3_ae7. The differences in $PM_{2.5}$ and SOA drivers between CRACMM and the two existing mechanisms are further explored. The results of this study provide a solid foundation for the further application of CRACMM in understanding and regulating air pollution in China and globally.

2. Methodology

2.1 Model configuration

Model simulations were conducted using CMAQ v5.4 with a horizontal resolution of 36 km × 36 km, covering mainland China (Figure 1). This domain includes five key city clusters with notable air pollution levels: Beijing-Tianjin-Hebei (BTH), Yangtze River Delta (YRD), Pearl River Delta (PRD), Fen-Wei Plain (FWP), and Sichuan Basin (SCB). Simulations were carried out for the months of January, April, July, and October 2021, representing winter, spring, summer, and autumn, respectively. The model includes 34 vertical layers, with the first layer located approximately 35 meters above the ground. Each simulation was initialized with a 15-day spin-up period before the start of each month. In addition to CRACMM version 1.0, two other chemical mechanisms, CB6r3_ae7 and Saprc07tic_ae7i, were included for comparisons, the number of reactions and gas- and particle-phase species in three different chemical mechanisms used in CMAQ are shown in Figure S1. All three mechanisms are available in CMAQ v5.4, with the "m3dry" deposition scheme selected. The initial and boundary conditions

https://doi.org/10.5194/egusphere-2025-3627
Preprint. Discussion started: 1 October 2025

for CRACMM and Saprc07tic_ae7i were mapped from the seasonal average hemispheric CMAQ output files distributed through the CMAS Data Warehouse. Meteorological input files were generated through an offline run of the Weather Research and Forecasting (WRF) model (https://www.mmm.ucar.edu/models/wrf) version 4.0 with configurations detailed in our previous studies (Huang et al., 2021a). The archived dataset, including the concentrations and model performance statistics of $PM_{2.5}$ and its components, model configurations, and the locations of all observation sites, is available on Zenodo (Su et al., 2025).

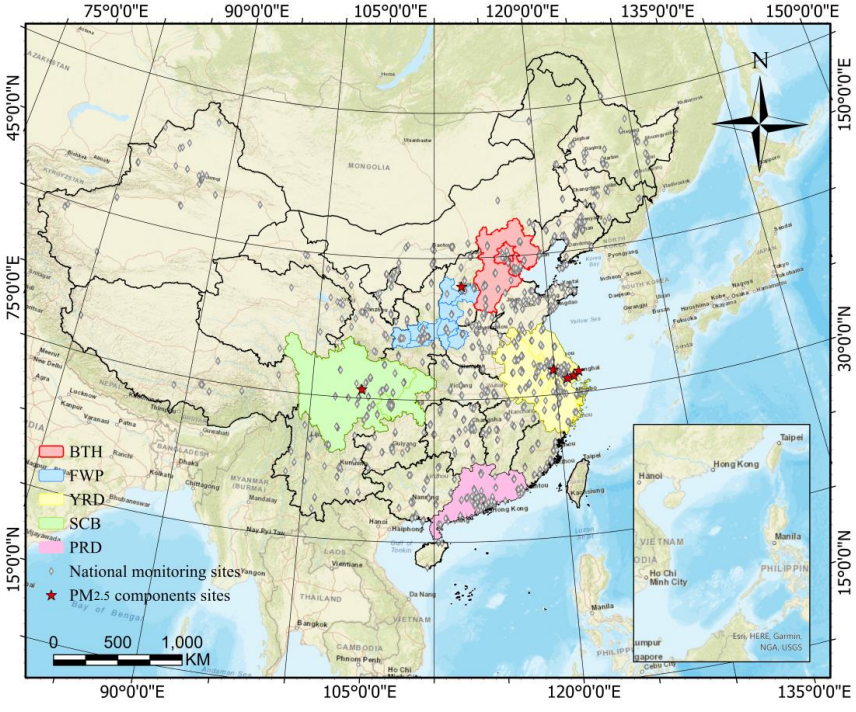

Figure 1. Model domain with five major city clusters (outlined in color), locations of national monitoring sites (grey diamonds), and six $PM_{2.5}$ chemical components observation sites (red stars).

2.2 Emissions

2.2.1 Traditional Emissions Inventory

The 2019 anthropogenic Multi-resolution Emission Inventory for China (MEIC), developed by Tsinghua University, was utilized in this study (http://www.meicmodel.org). Biogenic emissions were estimated using the Model of Emissions of Gases and Aerosols from Nature

https://doi.org/10.5194/egusphere-2025-3627
Preprint. Discussion started: 1 October 2025

version 3.2 (MEGANv3.2, https://bai.ess.uci.edu/megan/data-and-code/megan32) (Guenther et al., 2012). Currently, MEIC supports VOC emission only for both CB6r3_ae7 and Saprc07tic_ae7i, but not the CRACMM mechanism. Therefore, anthropogenic VOC species were converted to CRACMM input species using a binary decision tree approach. This approach distinguishes between one-to-one and non-one-to-one mappings based on chemical species correspondence from Saprc07tic_ae7i and CB6r3_ae7 to CRACMM. The one-to-one mappings are further classified into explicit one-to-one (routine A) and lumped one-to-one (routine B), while the non-one-to-one mappings include many-to-one (routine C) and many-to-many (routine D) cases. In routine A, both Saprc07tic_ae7i and CB6r3_ae7 consist of a few species that can be mapped directly to CRACMM based on CAS number, e.g., HCHO (formaldehyde) is mapped to HCHO. In routine B, the mapping is based on lumped species categories or names. For example, OLE1 (alkenes other than ethene, with kOH < 7×10^4 ppm^{-1} min^{-1}) in Saprc07tic_ae7i is mapped to OLI (internal alkenes) in CRACMM, OLE2 (alkenes with kOH > 7×10^4 ppm^{-1} min^{-1}) is mapped to OLT (terminal alkenes), and ONIT is mapped to RNO3 based on the same name used for organic nitrates.

In routine C, new species could be added to the CRACMM mechanism, such as CSL (Cresols) and PHEN (Phenol and aromatic diols), which correspond to CRES (phenols and cresols) in the Saprc07tic_ae7i mechanism. In this case, we use the emission factor ratio to distribute the species. As MEIC does not provide species-level emission factors, data from the 2017 U.S. National Emission Inventory (NEI) (Pye et al., 2023) were utilized, which contain over 3,000 species with corresponding emission factors, source sectors, and CRACMM species mappings. The emission factors are averaged over all sources for different MEIC sectors (mobile sources, industrial sources, etc.). Another example is that both XYE (P-xylene and less reactive aromatics) and XYM (M-xylene and more reactive aromatics) are newly introduced species in the CRACMM mechanism, corresponding to XYL (Xylene and other aromatics) in the Saprc07tic_ae7i mechanism. According to the 2017 NEI, their ratio is 0.3:0.7. Therefore, 0.3 of XYL in Saprc07tic_ae7i is assigned to XYE in CRACMM, and 0.7 of XYL in Saprc07tic_ae7i is assigned to XYM in CRACMM.

Routine D is more complicated, but the mapping is still based on the emission factor ratio for proper mapping. For instance, in CRACMM, GLY represents both glyoxal and glycolaldehyde.

https://doi.org/10.5194/egusphere-2025-3627
Preprint. Discussion started: 1 October 2025

To construct this species from Saprc07tic_ae7i, GLY (representing glyoxal only) and part of CCHO (glycolaldehyde and acetaldehyde) are mapped, such that GLY in CRACMM corresponds to GLY + CCHO × 0.25 in Saprc07tic_ae7i. Similarly, ACD (acetaldehyde) in CRACMM corresponds to CCHO × 0.75 in Saprc07tic_ae7i. For species lumped from multiple species, only those with larger emission factors are considered. Table S1 outlines the correspondence relationships for major species with substantial emissions. Since it is challenging to compare VOC emissions in different mechanisms due to the lumping rules, we only conducted an overall comparison of total emissions, as shown in Table S2.

2.2.2 POA Emissions

Two POA inventories were employed in this study: a traditional POA emissions inventory and a full volatility inventory. CRACMM, Saprc07tic_ae7i, and CB6r3_ae7 all use the same dataset for the traditional POA emissions inventory. This inventory applies a VBS profile based on Woody et al. (2016) and Robinson et al. (2007), treating POA as semi-volatile with C_i^* values ranging from 10^{-2} to 10^3 μg/m³. The detailed species of POA included in each mechanism are listed in Table S3.

In contrast, the full volatility inventory distributes POA emissions across a wider range of volatility bins. Laboratory experiments have demonstrated that L/S/IVOC emissions, which are largely absent in the traditional POA inventory, contribute to SOA formation much more efficiently than VOCs, owing to their lower volatility. To capture these processes, the full volatile inventory developed by Chang et al. (2022) was used, with species mapped from the two-dimensional VBS (2D-VBS) mechanism to CRACMM based on their C_i^* and O:C values. Since neither Saprc07tic_ae7i nor CB6r3_ae7 includes a representation of full volatile POA, only CRACMM can utilize this comprehensive inventory. The methodology outlined by Chang et al. (2022) includes emissions from various sources, along with their corresponding profiles, volatility ranges, and emission amounts. For traditional POA inventory, the POA emission amount was 2840 kt/y, while the new full volatile emission inventory includes emissions of LVOC (1,342 kt/y), SVOC (1,169 kt/y), and IVOC (3,939 kt/y), resulting in a total of 6,450 kt/y. The new inventory fills a gap of 3,610 kt/y in L/S/IVOC emissions that were absent from the traditional inventory. To thoroughly evaluate CRACMM and compare it with CB6r3_ae7 and Saprc07tic_ae7i, four simulation scenarios were designed, as shown in Table 1.

https://doi.org/10.5194/egusphere-2025-3627
Preprint. Discussion started: 1 October 2025

Additionally, the empirical representation of anthropogenic SOA source (pcSOA) (Murphy et al., 2017) was turned off in CB6r3_ae7 and Saprc07tic_ae7i, as pcSOA is deprecated in CRACMM.

Table 1. Description of simulation scenarios and their emissions

Scenarios	Mechanisms	POA emission inventory	Anthropogenic + Biogenic emission inventory
1	CB6r3_ae7	Traditional POA inventory	MEIC+MEGAN
2	Saprc07tic_ae7i	Traditional POA inventory	MEIC+MEGAN
3	CRACMM	Traditional POA inventory	MEIC+MEGAN
4	CRACMM	Full volatile inventory	MEIC+MEGAN

2.3 Observational data and model performance evaluation

Hourly concentrations of $PM_{2.5}$ at national monitoring stations were obtained from the China National Environmental Monitoring Centre (http://air.cnemc.cn:18007), which were then used to evaluate model performance. Field observational data of $PM_{2.5}$ chemical components including NO_3^- (nitrate), SO_4^{2-}, NH_4^+ (ammonium), OC (organic carbon), and EC (elemental carbon) at six super monitoring station sites were collected, as detailed in Figure 1 and Table S4. Missing observation periods were excluded from the analysis. Model performance was assessed using well-established statistical metrics, including the R, MB, NMB, root mean square error (RMSE), normalized mean error (NME), and index of agreement (IOA). The equations for calculating these metrics can be found in our previous study (Wang et al., 2024; Huang et al., 2021a).

3. Results and discussion

3.1 Overview of CMAQ-CRACMM model performance evaluation on $PM_{2.5}$

Figure 2 depicts the spatial distribution of observed (dots) and simulated $PM_{2.5}$ concentrations for January, April, July, and October 2021, based on the CRACMM model with the full volatile inventory. In January (Figure 2a), $PM_{2.5}$ concentrations range from 5 to over 100 μg/m³, with the highest values concentrated in the North China Plain (NCP) and parts of the SCB. These elevated levels are primarily driven by relatively higher anthropogenic emissions and stagnant

https://doi.org/10.5194/egusphere-2025-3627
Preprint. Discussion started: 1 October 2025

meteorological conditions typical of winter. In April (Figure 2b), concentrations have significantly decreased, ranging from 5 to 40 μg/m³, with the most notable reductions observed in northern regions. During July (Figure 2c), $PM_{2.5}$ concentrations were at their lowest, typically ranging from 0 to 40 μg/m³. This decline is mainly attributable to the increased precipitation and the associated washout of pollutants. In addition, higher planetary boundary layer (PBL) heights during the warm season, coupled with enhanced atmospheric mixing and dilution, further contributed to the decrease in $PM_{2.5}$ concentrations. In October (Figure 2d), $PM_{2.5}$ concentrations rise again, ranging from 5 to 60 μg/m³, with the highest concentrations observed in the NCP and along the eastern coastal regions, which is attributed to the heating in later autumn and unfavorable meteorological conditions. Overall, monthly variations in $PM_{2.5}$ concentrations are primarily driven by meteorological conditions and the distribution of emission sources.

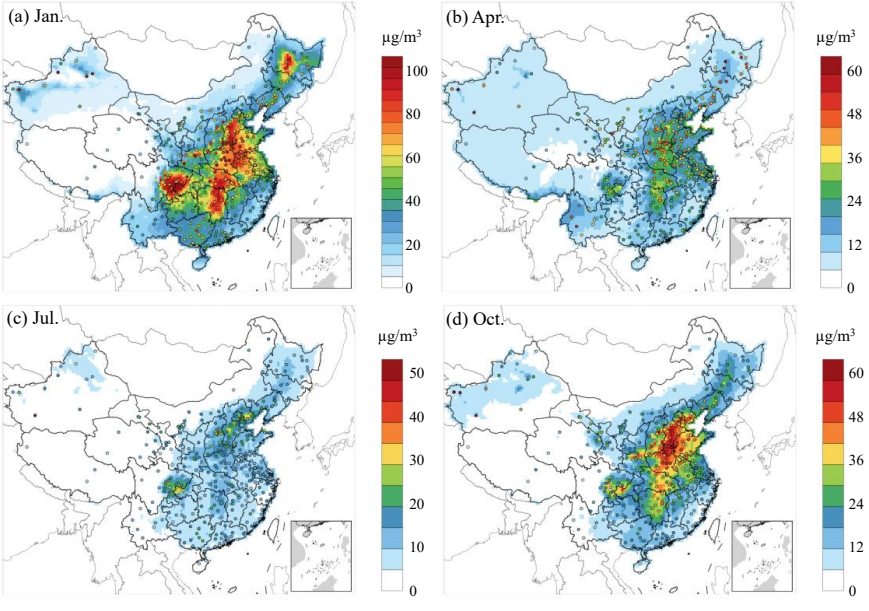

Figure 2. Monthly average $PM_{2.5}$ concentrations predicted (raster) by CRACMM and observed (dots) in 2021 using the full volatility emission inventory.

The performance of the CMAQ model in simulating hourly $PM_{2.5}$ concentrations was evaluated by comparing the model outputs with observations from national monitoring sites. In January, CRACMM exhibited generally high R values in Northern China, indicating strong agreement

https://doi.org/10.5194/egusphere-2025-3627
Preprint. Discussion started: 1 October 2025

between observed and simulated $PM_{2.5}$ levels. In contrast, lower R values were observed in southern regions. The model demonstrated a negative bias across most areas (Figure 4a), suggesting a general underestimation of $PM_{2.5}$ concentrations, except in the YRD and SCB regions, where positive biases are observed at many sites. This discrepancy is likely due, in part, to the frequent dust storm events in January of that year. Although both observations and model outputs from the major dust episodes on January 13–14 were excluded to minimize their influence on the monthly evaluation, the missing of dust emissions, the complex meteorological conditions associated with persistent northern dust layers may have contributed to an underestimation of $PM_{2.5}$ concentrations by up to 30 μg/m³ in northern regions. Nevertheless, the model still achieves high R values in the BTH, YRD, and FWP regions.

Results for April (Figures 3b and 4b) show generally strong correlations in the eastern regions, while several monitoring sites in the south exhibit lower R values. Compared to January, the MB is less pronounced. April also experiences dust storm events. In July, R values decline across all regions relative to January and April, and most stations exhibit relatively small MB values (Figures 3c and 4c). The strong influence of temperature and solar radiation on photochemical processes during summer may result in more pronounced diurnal variations in chemical composition, making the simulation of chemical processes more challenging. Moreover, the chemical mechanisms may inadequately capture non-linear interactions and the influence of SOA, further reducing the correlation. Additionally, synoptic-scale variations can also affect the spatial distribution and concentration of key atmospheric species. R values are improved in October (Figures 3d and 4d), with 90% of the sites achieving R values of 0.8 and the MB is around 10 μg/m³ with higher evaluation in SCB and BTH regions. Overall, wintertime observed peaks generally underestimated and lower summertime observed values generally captured. The model demonstrates strong performance in January and October, characterized by higher correlations and smaller biases. However, it had weaker performance in April and July with lower correlations.

https://doi.org/10.5194/egusphere-2025-3627
Preprint. Discussion started: 1 October 2025

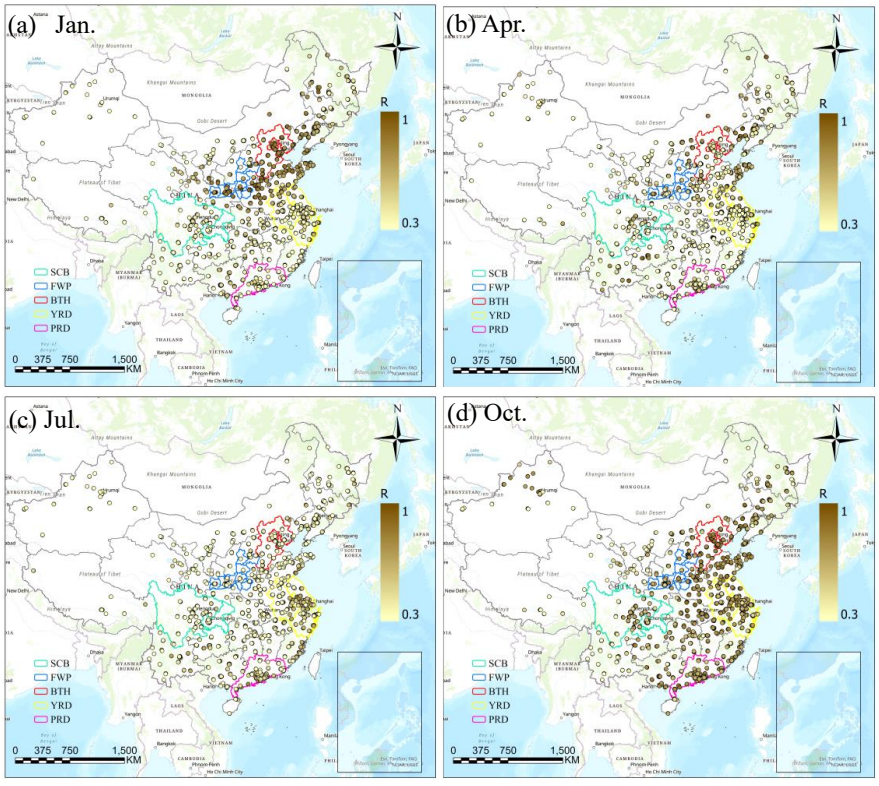

Figure 3. R values between predicted and observed $PM_{2.5}$ concentrations using CRACMM with the full volatile emission inventory for January, April, July, and October of 2021.

Figures S2 and S3 compare the R and MB values between CRACMM (with the full-volatile inventory) and CB6r3_ae7 (with the traditional inventory). In January, CRACMM demonstrates notable improvements in R values at several sites in the PRD and YRD regions, with increases ranging from 0.2 to 0.4 (Figure S2a), while changes at most other sites remain relatively minor. Regarding MB, the most pronounced differences also occur in January: some locations in the BTH and YRD regions show higher MB values—up to 10 μg/m³—with CRACMM, whereas other regions display reduced MB values (Figure S3a). In April (Figures S2b and S3b), CRACMM achieves higher R values at certain sites in the YRD, while slightly lower correlations are observed in the PRD compared to CB6r3_ae7. MB values remain elevated in the SCB and parts of the YRD region for CRACMM. For July (Figures S2c and S3c), R values from CRACMM are generally comparable to those from CB6r3_ae7. However, MB values tend to decrease across most regions, indicating a potential improvement in bias

https://doi.org/10.5194/egusphere-2025-3627
Preprint. Discussion started: 1 October 2025

performance during summer. In October, CRACMM shows moderate increases in R values—by approximately 0.1 at most sites (Figure S2d). MB values are lower in the PRD region but higher in the FWP region compared to CB6r3_ae7 (Figure S3d).

In evaluating the CMAQ model's performance for hourly $PM_{2.5}$ concentrations, CRACMM generally shows good correlations with observed data in January and October. However, discrepancies arise in April and July, likely due to complex meteorological and chemical conditions such as dust storms and increased photochemical activity. The model tends to underestimate peak $PM_{2.5}$ concentrations during winter but captures lower summer concentrations more accurately. Comparisons between CRACMM (with the full-volatile inventory) and CB6r3_ae7 (using the traditional inventory) highlight improvements in R values in the PRD and parts of the YRD regions in January for CRACMM, although performance declines in July.

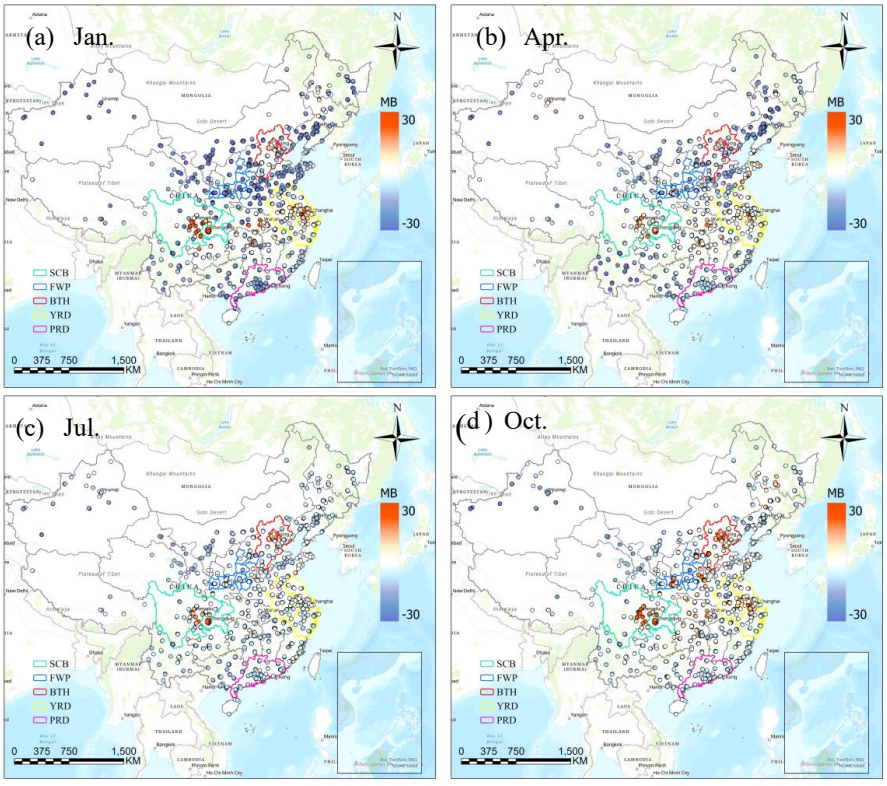

Figure 4. The MB values between predicted and observed $PM_{2.5}$ concentrations using CRACMM with full volatile inventory for January, April, July, and October of 2021.

https://doi.org/10.5194/egusphere-2025-3627
Preprint. Discussion started: 1 October 2025

$PM_{2.5}$ components in six selected cities using CRACMM with the full volatile inventory were evaluated. The data of certain cities have been used in previous studies(Wang et al., 2024). Details for the selected cities are provided in Table S4, Tables S5-S8 present the statistical performance of $PM_{2.5}$ components—including NO_3^-, SO_4^{2-}, NH_4^+, OC, and EC—across four months. Figures S7-S10 demonstrate that CRACMM effectively captured the overall peaks and troughs of observed $PM_{2.5}$ concentrations in January. The model also successfully simulated the heavy pollution period from January 20th to 25th in Taiyuan, with results similar to our previous study (Wang et al., 2024). The three ions were well simulated in both Changzhou and Pudong in the YRD region, particularly in Changzhou, where the overall trends of OC and EC showed strong consistency with observations. However, for EC in Pudong, the model struggled to capture the hourly peak values accurately.

Table 2. Monthly averaged metrics of $PM_{2.5}$ evaluation and the number of monitoring sites.

Months	R	IOA	NMB	NME	No.
January	0.46	0.61	-18.58%	43.23%	1388
April	0.41	0.52	-29.07%	47.39%	1402
July	0.36	0.49	-32.39%	42.59%	1309
October	0.68	0.72	-11.48%	44.95	1358
Recommend benchmark	>0.60	>0.70	<±45%	<±55%	/

As shown in Table 2, based on observations from over 1,300 monitoring sites across China for CRACMM, the correlation metrics (R and IOA) met the recommended benchmark (Huang et al., 2021b) in October, while they fell short of the benchmark in January, April, and July. In contrast, the bias metrics (NMB and NME) satisfied the recommended benchmark across all four representative months, indicating that the model performed well in controlling overall bias. The evaluation metrics for different regions and months are provided in Tables S9–S12.

The heatmaps in Figure S4 illustrate the variations in R values across the five key regions—YRD, SCB, PRD, FWP, and BTH—for the three chemical mechanisms over four representative months (January, April, July, and October). Corresponding heatmaps for MB and NMB are presented in Figures S5 and S6, respectively.

In the YRD region, all mechanisms show relatively stable R values across the four months (Figure S4). The CRACMM simulation using the traditional inventory consistently results in lower MB (Figure S5) and NMB (Figure S6) values compared to CB6r3_ae7 and

https://doi.org/10.5194/egusphere-2025-3627
Preprint. Discussion started: 1 October 2025

Saprc07tic_ae7i throughout the year. When the full volatile inventory is incorporated, MB improves in April and July but worsens in January and October. Similarly, NMB values indicate higher modeled concentrations in all four months with the full volatile inventory compared to the traditional one. This trend is consistent with Figures S5, and 5, where the YRD region shows higher modeled concentrations from CRACMM using the full volatile inventory than from both CB6r3_ae7 and Saprc07tic_ae7i across all months.

In the SCB region, R values remain relatively consistent across the three mechanisms (Figure S4a–c). A slight improvement is observed in July, where R increases from 0.22 with the traditional inventory to 0.27 with the full volatile inventory (Figure S4d). However, in October, R decreases from 0.62 to 0.56 after switching to the full volatile inventory. The increase in R value in July suggests that the traditional inventory may underestimate key precursors (e.g., S/IVOCs), while the full-volatility inventory better captures these species active at higher temperatures, improving model–observation agreement. In contrast, the October decrease in R may reflect uncertainties in representing some gas- or particle-phase organics under cooler conditions. Regarding MB, CRACMM generally shows reduced values in most months when using the traditional inventory, except for April. With the full volatile inventory, MB decreases further in October, while slight increases are observed in the other months. The trends in NMB follow a similar pattern to those in MB. It could be due to overestimation of certain intermediate- or low-volatility species under specific conditions.

In the PRD region, CRACMM exhibits notable performance improvements in January. As shown in Figures S4a–c, the R value increases from 0.20 with CB6r3_ae7 and Saprc07tic_ae7i to 0.35 when using CRACMM with the traditional POA inventory. When the full volatile inventory is applied (Figure S4d), the R value further increases to 0.50. Concurrently, the MB improves significantly, decreasing from –19.6 μg/m³ to –11.8 μg/m³, and the NMB is reduced from –43% to –26%. These results indicate that CRACMM, particularly with the full volatile inventory, achieves both higher correlation and lower bias for $PM_{2.5}$ simulations in the PRD region during January. Under the traditional POA inventory, CRACMM tends to underestimate $PM_{2.5}$ concentrations in PRD during January (Figure S3a). However, after switching to the full volatile inventory, simulated concentrations exceed those predicted by CB6r3_ae7 (Figure 5a), primarily due to increased contributions from SOA (Figure 8b). In comparison, during April

https://doi.org/10.5194/egusphere-2025-3627
Preprint. Discussion started: 1 October 2025

and July, the CRACMM simulations using the traditional emissions inventory showed lower R values than those of CB6r3_ae7 and Saprc07tic_ae7i, and the correlation further declined when using the full-volatility emissions inventory. Although CRACMM features a more comprehensive design for gas-phase oxidation mechanisms, the intense photochemical activity in July and the rapid oxidation of high concentrations of IVOC precursors may have introduced more complex SOA formation pathways and product distributions, thereby increasing modeling uncertainties and weakening the agreement with observations. By October, model performance had improved. Across all months, CRACMM combined with the full-volatility emissions inventory consistently outperformed the other mechanisms in terms of MB and NMB, highlighting the critical role of this inventory in addressing the underestimation of $PM_{2.5}$ associated with traditional POA treatment.

In the FWP region, both the R (Figure S4a–c) and MB (Figure S5a–c) values show minimal variation across the three mechanisms, indicating limited sensitivity to the chemical mechanism alone. However, notable changes in MB and NMB are observed with the incorporation of the full volatile inventory in April, July and October, which align with the higher $PM_{2.5}$ concentrations shown in Figure 5, compared to CB6r3_ae7. In April and July, MB values shift from -12.7 μg/m³ and -5.6 μg/m³ to -2.4 μg/m³ and 1.2 μg/m³, respectively, with NMB showing a similar trend. These changes suggest an improvement in model agreement when the full volatile inventory is employed. In contrast, both MB and NMB increase in October, indicating that the full volatile inventory leads to higher simulated concentrations during this month.

In the BTH region, The R (Figure S4a–c) and MB (Figure S5a–c) values remain largely consistent across the three mechanisms. CRACMM with the traditional POA inventory shows a decrease in R values from 0.44 to 0.38 compared to CB6r3_ae7 in July. After incorporating the full volatile inventory, the R in BTH experiences a more significant drop, falling to 0.24. Notably, MB and NMB indicate that the modeled results are lower for CRACMM with the traditional POA inventory in January, while they are higher in the other months. Additionally, BTH exhibited the highest IVOC emissions in the inventory (Chang et al., 2022), and uncertainties in emission estimates may have further contributed to this result.

Overall, the differences in R and MB values across the three chemical mechanisms are relatively small when the traditional POA inventory is used. However, for CRACMM, the MB

https://doi.org/10.5194/egusphere-2025-3627
Preprint. Discussion started: 1 October 2025

in January indicates a stronger underestimation, primarily due to differences in POA (as shown in Figure 8a), leading to lower modeled concentrations compared to CB6r3_ae7 and Saprc07tic_ae7i. With the incorporation of the full volatile inventory, the MB shifts toward higher modeled concentrations in the subsequent three months. Notably, more pronounced differences are observed in January in the PRD region and in July in the BTH region.

3.2 Comparisons of model predicted $PM_{2.5}$ between CRACMM and other mechanisms

Figures 5 and 6 illustrate the differences in model outputs between CRACMM with full volatile inventory and CB6r3_ae7, as well as between CRACMM and Saprc07tic_ae7i. In January, CRACMM predicts lower $PM_{2.5}$ concentrations across central and northern China compared to both CB6r3_ae7 (Figure 5a) and Saprc07tic_ae7i (Figure 6a), with the differences—up to 10 $\mu g/m^3$—observed in central and north of China. While CRACMM simulates higher $PM_{2.5}$ concentrations in the PRD and YRD regions. For the remaining months—April, July, and October—CRACMM with full volatile inventory generally predicts higher $PM_{2.5}$ levels than the other two mechanisms (Figures 5b–d, Figures 6b–d). When CRACMM and CB6r3_ae7 are configured with the traditional POA inventory, as shown in Figure S11, the differences of $PM_{2.5}$ concentrations are reduced in April, July, and October compared with full volatile POA inventory. But CRACMM still predicts lower $PM_{2.5}$ levels than CB6r3_ae7 in January. A likely explanation is that the lower photochemical activity leads to reduced SOA formation, as the enhanced SOA pathways are less active during the winter months.

https://doi.org/10.5194/egusphere-2025-3627
Preprint. Discussion started: 1 October 2025

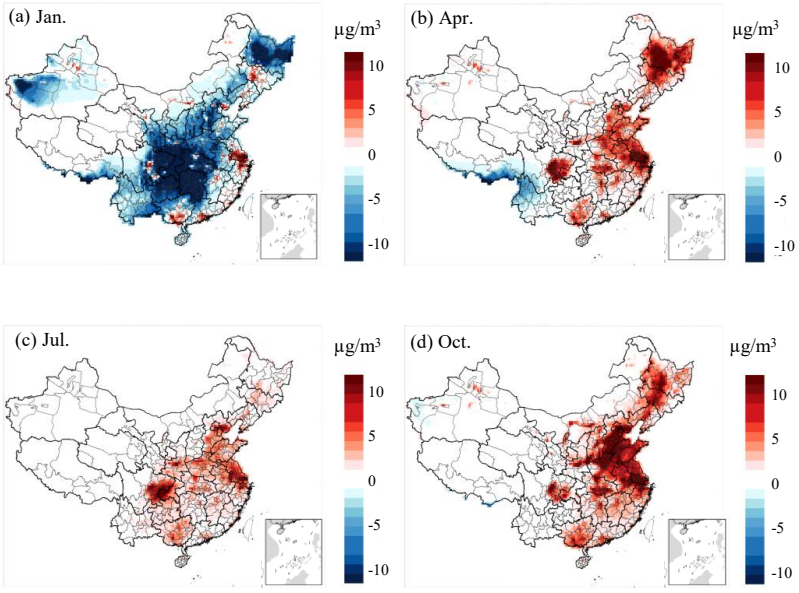

Figure 5. Differences in model-predicted $PM_{2.5}$ concentrations between CRACMM（full volatile inventory) and CB6r3_ae7.

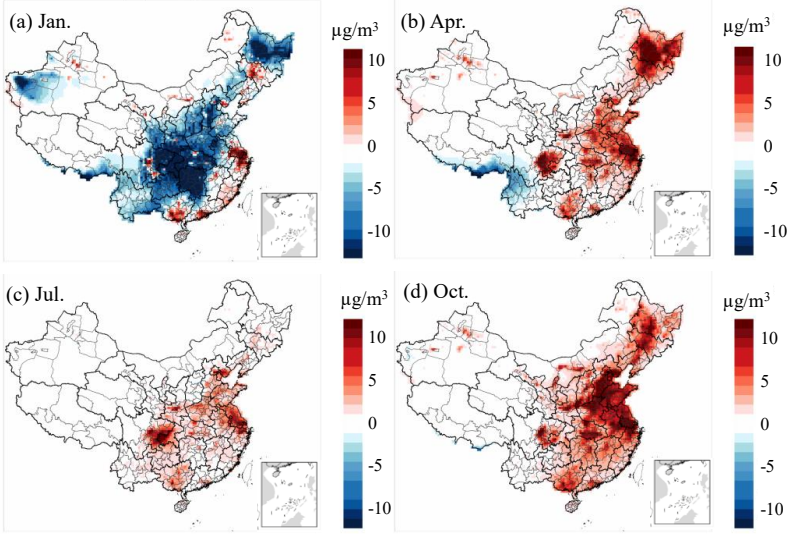

Figure 6. Differences in model-predicted $PM_{2.5}$ concentrations between CRACMM（full volatile inventory) and Saprc07tic_ae7i.

https://doi.org/10.5194/egusphere-2025-3627
Preprint. Discussion started: 1 October 2025

3.3 Comparisons of model predicted $PM_{2.5}$ chemical components between CRACMM and other mechanisms

Analysis of Figures 5, 6, and S11 indicates that the most significant differences among the model simulations occur in January and October, whereas the discrepancies between chemical mechanisms are substantially smaller in April and July—likely due to the overall lower pollutant concentrations during these months, which may reduce the sensitivity to mechanistic differences. Consequently, the subsequent analysis focuses on a detailed comparison of $PM_{2.5}$ component variations between CRACMM and CB6r3_ae7 for January and October.

3.3.1 Inorganic aerosol

SO_4^{2-}, NO_3^-, and NH_4^+ are the dominant secondary inorganic components in $PM_{2.5}$. Nitrogen dioxide (NO_2) and sulfur dioxide (SO_2) can fully dissolve into cloud water or aerosol liquid phases and subsequently oxidize to form nitrate and sulfate. Ammonium salts are produced through the neutralization reactions of these acidic species with atmospheric ammonia (NH_3). EC primarily originates from the incomplete combustion of carbonaceous fuels, especially under oxygen-limited conditions. It is commonly emitted from sources such as vehicle exhaust, industrial combustion, and biomass burning. From a chemical mechanism perspective, CRACMM retains the inorganic chemistry framework of RACM2 but incorporates updated rate constants for several reactions. Specifically, the rate expressions for 26 inorganic reactions were revised in CRACMM compared to RACM2 (Pye et al., 2023). Overall, differences in inorganic component predictions among CRACMM, CB6r3_ae7, and Saprc07tic_ae7i are relatively minor. As shown in Figure 7, predicted concentrations of major inorganic species in January and October are comparable between CRACMM and CB6r3_ae7, with differences ranging from −1 to 1 μg/m³ for EC and SO_4^{2-}, and −5 to 5 μg/m³ for NH_4^+ and NO_3^-. These results suggest that the variation in simulated inorganic aerosol concentrations is only marginally affected by differences in the inorganic chemistry schemes.

https://doi.org/10.5194/egusphere-2025-3627
Preprint. Discussion started: 1 October 2025

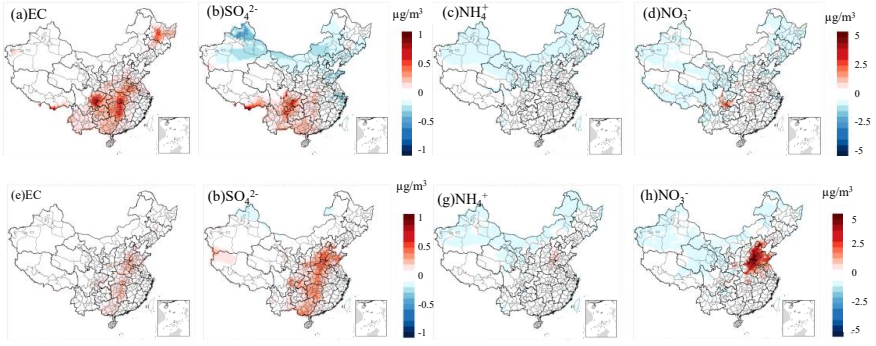

Figure 7. Differences in model-predicted $PM_{2.5}$ components—(a)EC, (b)SO_4^{2-}, (c)NH_4^+, (d)NO_3^- for January, and (e)EC, (f)SO_4^{2-}, (g)NH_4^+, (h)NO_3^- for October—between CRACMM (with full volatile inventory) and CB6r3_ae7. Figures (a–d) share the same scale, as do figures (e–h).

3.3.2 Organic aerosol

In January, CB6r3_ae7 consistently predicts higher POA concentrations than CRACMM under both the traditional and full-volatile inventory configurations, with the most pronounced differences occurring in east China (Figure 8a and Figure S12a). In CRACMM, POA aging is represented using a modified 2D-VBS framework (Murphy et al., 2017), where C_i^* range from 10^{-2} to 10^3 μg/m³. A significant portion of the alkane-like L/SVOC mass contributing to ambient OA comes from the direct emissions of low-volatility species (e.g., AROCN2ALK, AROCN1ALK, AROCP0ALK, AROCP1ALK, AROCP2ALK, AROCP3ALK) and their oxidation products (e.g., ROCN2OXY2, ROCP0OXY2, ROCP1OXY1, ROCP2OXY2, ROCP3OXY2). By contrast, CB6r3_ae7 adopts a semi-volatile POA approach in which primary emissions (e.g., LVPO1, SVPO1–3, IVPO1) and their oxidation products (e.g., (LVOO1, LVOO2, SVOO1, SVOO2, SVOO3) partition between gas and particle phases across a C_i^* range of 10^{-1} to 10^3 μg/m³. This framework aligns with the 1.5D-VBS scheme proposed by Koo et al. (2014). Details of the POA species and their properties are provided in Table S3. The most significant differences in simulated POA concentrations occur in January, likely due to enhanced partitioning of SVOC to the particle phase under low wintertime temperatures. Additionally, differences in multigenerational oxidation aging and volatility treatment between

https://doi.org/10.5194/egusphere-2025-3627
Preprint. Discussion started: 1 October 2025

the two mechanisms contribute to the simulation discrepancies. In October, although POA concentrations in CRACMM remain lower than in CB6r3_ae7, the difference is less pronounced compared to January for both POA inventory (Figures 8e and S12e).

To better understand the drivers of SOA formation in the two mechanisms, we analyzed the spatial distribution of SOA concentrations under both traditional and full-volatile POA inventories. In January, CRACMM predicts higher SOA levels in the BTH and parts of the SCB regions compared to CB6r3_ae7 when using the traditional POA inventory (Figure S12b). Under the full-volatile inventory, CRACMM also shows increased SOA concentrations in the YRD and PRD regions (Figure 8b). These increases correspond with high IVOC emissions in BTH and YRD, consistent with the spatial patterns reported by Chang et al. (2022), although their data reflect monthly averages across January and July. The SOA enhancement in YRD and PRD under the full-volatile inventory highlights the critical role of IVOC emissions in these areas. In CB6r3_ae7, SOA is primarily formed from the oxidation of traditional VOC sources, such as isoprene, monoterpenes, sesquiterpenes, benzene, toluene, xylene, alkanes, and PAHs (Carlton et al., 2010; Pye and Pouliot, 2012).

In contrast, CRACMM incorporates additional SOA precursor systems, including phenol and aromatic diols, pinon aldehyde, oxygenated IVOCs, furanone, and other compounds. As a result, in regions with elevated anthropogenic emissions, CRACMM generally simulates higher SOA concentrations. However, in the SCB region, SOA levels remain lower, possibly due to the reduced reactivity of these new precursors under the lower ambient temperatures typical of this region. In terms of overall OA concentrations, CRACMM generally predicts lower values than CB6r3_ae7 across most regions, except for some part of YRD region (Figure 8c and Figure S12c). The spatial distribution of OC is similar to that of OA, with CRACMM also showing lower concentrations than CB6r3_ae7 (Figure 8d and Figure S12d).

In October (Figures 8f–h and S12f–h), SOA remains the dominant contributor to the differences in $PM_{2.5}$ concentrations. Under the full-volatile inventory, CRACMM predicts significantly higher SOA concentrations compared to CB6r3_ae7 (Figure 8f), resulting in elevated OA levels (Figure 8g). The spatial pattern of OC concentrations (Figure 8h) closely resembles that of OA. When the traditional POA inventory is applied, the differences in SOA, OC, and OA concentrations between the two mechanisms are minimal (Figures S12f–h). The most

https://doi.org/10.5194/egusphere-2025-3627
Preprint. Discussion started: 1 October 2025

pronounced increases with the full-volatile inventory are observed in the YRD, PRD, and SCB regions, attributable to the inclusion of a more comprehensive set of SOA precursors.

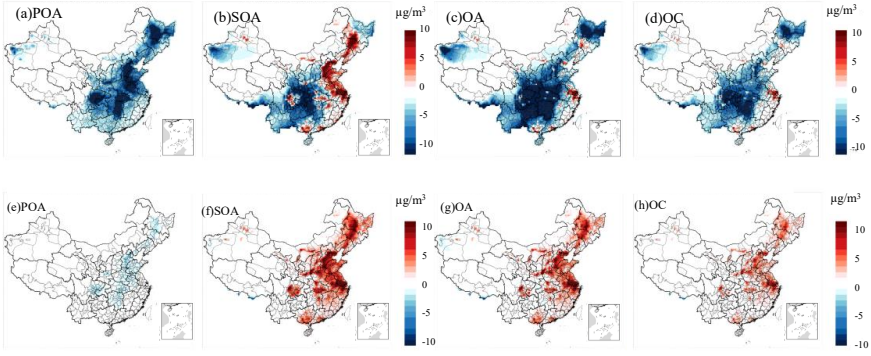

Figure 8. Differences in model-predicted $PM_{2.5}$ components—(a) POA, (b) SOA, (c) OA, and (d) OC for January, and (e) POA, (f) SOA, (g) OA, and (h) OC for October—between CRACMM (with full volatile inventory) and CB6r3_ae7. Figures (a–d) share the same scale, as do figures (e–h).

Overall, in January, the primary differences between CRACMM and CB6r3_ae7 stem from lower POA concentrations in CRACMM, primarily due to semi-volatile partitioning and reduced aging of semi-volatile POA species at lower temperatures. SOA concentrations are elevated in eastern China but reduced over the SCB, reflecting both the slower oxidation of additional SOA precursors under winter conditions in the SCB and the greater availability of these precursors in the eastern region. In October, the key differences in model predictions are primarily driven by the POA inventory used. The full-volatility inventory yields higher SOA concentrations than the traditional inventory, largely due to the inclusion of L/S/IVOCs, which are efficient SOA precursors.

3.4 Sensitivity study on $PM_{2.5}$ and SOA responses to changes of precursors

In this section, CMAQ simulations with emission perturbations are conducted to identify the key drivers of $PM_{2.5}$ formation in January, when $PM_{2.5}$ concentrations are notably high. A series of emission sensitivity simulations were performed within CMAQ to assess the role of precursor ROC systems in $PM_{2.5}$ formation using CRACMM with the full volatile inventory across China. These sensitivity simulations involved running zeroed emission scenarios for

https://doi.org/10.5194/egusphere-2025-3627
Preprint. Discussion started: 1 October 2025

January (i.e., setting emissions of a specific chemical class or sector to zero) to examine how $PM_{2.5}$ concentrations respond to changes in emissions. A subset of these sensitivity simulations was also conducted using the CB6r3_ae7 and Saprc07tic_ae7i mechanisms. A detailed list of all the zeroed emission simulations is provided in Tables 3 and S13. Due to the non-linear nature of $PM_{2.5}$ production in response to ROC perturbations, these simulations offer an initial evaluation of how $PM_{2.5}$ formation responds to reduced ROC emissions, providing valuable insights into how chemical systems behave under varying emission conditions in the three mechanisms.

Table 3. List of emission reductions relative to the base simulations in CMAQ-CRACMM.

Chemical Mechanism	Emission Reduction
CRACMM	Benzene, toluene and xylene-like emissions set to zero
CRACMM	Biogenic-ROC emissions set to zero
CRACMM	IVOC emissions set to zero
CRACMM	SVOC emissions set to zero
CRACMM	HC10 zero out (decane and species of similar reactivity)

Figure 9 shows domain-wide differences in average $PM_{2.5}$ concentrations between the base CRACMM simulation and a series of zeroed emission simulations. A similar spatial pattern in $PM_{2.5}$ response was observed for zeroed biogenic and HC10 emissions (Figures S13a, c in percentage and Figures 9a, c in concentration), with CRACMM predicting a modest 1% change in $PM_{2.5}$ and less than 3 $\mu g/m^3$ in many parts of China. This can be attributed to the low SOA yield by mass (0.09 g/g) for HC10 compounds (Pye et al., 2023), and the generally low winter emissions of biogenic ROC, as shown in previous studies (Pye et al., 2023). Zeroing BTX emissions resulted in average $PM_{2.5}$ concentration changes of -20% to 0% (Figure S13b) and -10 to 0 $\mu g/m^3$ (Figure 9b), particularly in the YRD and BTH regions, where BTX emissions are highest. The high $PM_{2.5}$ formation potential of BTX compounds is attributed to their overall emission abundance and high SOA yield by mass (~0.5 g/g). Moreover, ozone levels in urban areas with significant BTX emissions also decrease in the BTX zero-out scenario (Figure S14). This effect is particularly evident in the PRD region, where the reduction reaches up to 10 $\mu g/m^3$. This aligns with the findings of Place et al. (2023). One factor is the removal of BTX emissions, which serve as precursors for SOA formation. The second factor is that zeroing BTX emissions leads to a decrease in O_3, which weakens atmospheric oxidizing capacity and reduces SOA

https://doi.org/10.5194/egusphere-2025-3627
Preprint. Discussion started: 1 October 2025

formation. However, it is important to note that Place's study was conducted in summer.

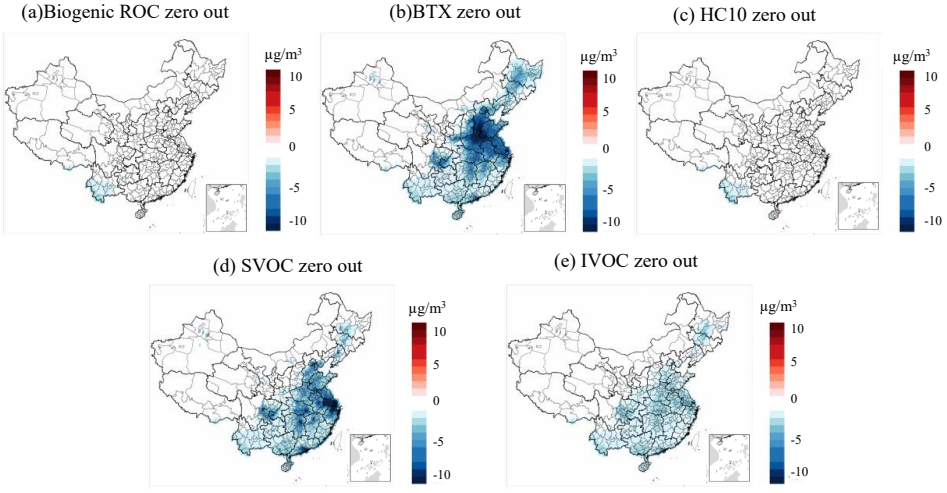

Figure 9. Changes in $PM_{2.5}$ concentrations between each zero-out scenario and its corresponding base simulation: (a) biogenic ROC emission, (b) BTX emission, (c) HC10 emission, (d) SVOC emission, and (e) IVOC emission with CRACMM.

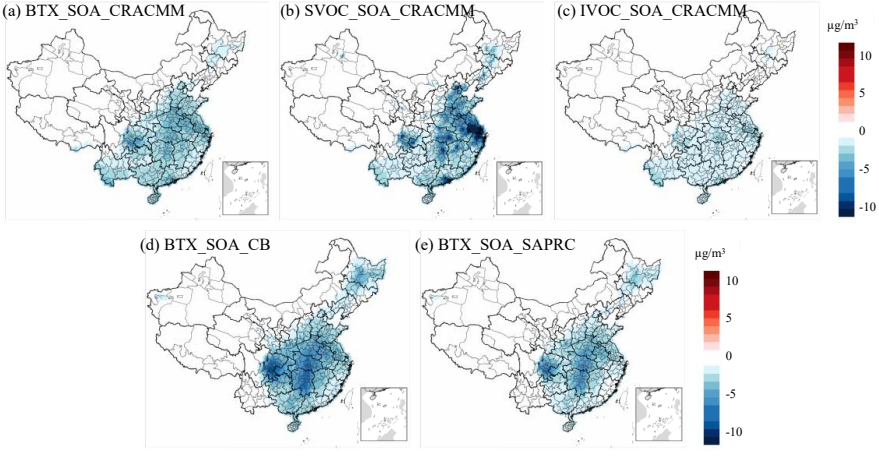

Figure 10. Changes in SOA concentrations between each zero-out scenario and its corresponding base simulation: (a) BTX emissions, (b) SVOC emissions, (c) IVOC emissions with CRACMM, (d) BTX emissions with CB6r3_ae7, (e) zeroed BTX emissions with Saprc07tic_ae6.

As shown in Figures 10a, d, and e, the impact of zeroing BTX species on SOA formation for the three mechanisms accounts for only approximately 50% of the total $PM_{2.5}$ change observed

https://doi.org/10.5194/egusphere-2025-3627
Preprint. Discussion started: 1 October 2025

in Figures 9b, S16a and c. This suggests that the changes in $PM_{2.5}$ concentrations resulting from the removal of BTX emissions are not solely due to SOA formation but may also involve other pathways or chemical processes. In contrast, the influence of S/IVOC species on $PM_{2.5}$ concentrations in the CRACMM mechanism is primarily driven by SOA formation. This conclusion is supported by the spatial distribution and concentration differences shown in Figures 9d, e, and Figures 10b, c, which exhibit nearly identical patterns. These similarities indicate that the effects of S/IVOC emissions on $PM_{2.5}$ are mainly driven by SOA production. The largest $PM_{2.5}$ response was observed when emissions from SVOC sources were excluded from the simulation (Figure S13d), primarily because SVOCs have the highest yield, exceeding 1.0 g/g. The percentage changes in $PM_{2.5}$ range from −40% to 0%, with a concentration reduction of more than −10 μg/m³ (Figure 9d), particularly in the YRD region, where SVOC emissions are substantial. For IVOCs, the reduction is about −5% across much of China, except in the western regions where IVOC emissions are very low (Figure S13e), resulting in a reduction of less than −5 μg/m³ (Figure 9e).

A similar $\Delta PM_{2.5}$ response in percentage (Figure S15) and concentration change (Figure S16) was observed when biogenic and BTX emissions were zeroed in simulations using CB6r3_ae7_ae7 and Saprc07tic_ae7i. However, the CRACMM simulation with zeroed biogenic emissions (Figure 9a) showed a more pronounced and widespread decrease in $PM_{2.5}$ compared to both CB6r3_ae7_ae7 and Saprc07tic_ae7i. This difference can be attributed to the inclusion of new S/IVOC species in MEGAN, which are not accounted for in the other two mechanisms. Additionally, zeroing BTX emissions had a greater impact in CB6r3_ae7, particularly in central China, compared to Saprc07tic_ae7i and CRACMM. A possible reason for this is that CRACMM reduces the number of lumped species in BTX and enhances the representation of aromatic IVOC species, such as single-ring aromatics $\log_{10}(Ci*)$ ≈5 (ROCP5ARO) and $\log_{10}(Ci*)$ ≈6 (ROCP6ARO). These species are included in CB6r3_ae7 under categories like m-xylene and other more reactive aromatics (XYM), as well as less reactive aromatics (XYE). As a result, CRACMM incorporates fewer species in BTX emissions compared to CB6r3_ae7.

3.5 Uncertainty Analysis and limitations

3.5.1 Limitations of VOC Speciation Mapping

https://doi.org/10.5194/egusphere-2025-3627
Preprint. Discussion started: 1 October 2025

In the speciation mapping process, explicit species were directly mapped across the CRACMM, CB6r3_ae7, and Saprc07tic_ae7i mechanisms, as these species are explicitly represented and therefore allow for one-to-one mapping. Consequently, their spatial distributions were assumed to be identical across the three mechanisms, and uncertainties associated with their emission estimates were considered negligible. In contrast, lumped species present greater complexity due to differences in the VOC species included within each lumped mechanism species. Given that a direct one-to-one mapping between lumped species is not feasible, the mapping was performed by matching the dominant lumped VOC species across mechanisms based on their relative emission magnitudes. Overall, CRACMM incorporates a more comprehensive set of VOC species than either CB6r3_ae7 or Saprc07tic_ae7i. The total mapped emissions associated with each mechanism-specific inventory are summarized in Table S2. Nevertheless, uncertainties remain due to regional differences in emission profiles. In particular, the total emissions and source sector distributions of VOC species in Chinese emission inventories may differ from those represented in the NEI. Such discrepancies introduce additional uncertainty into the speciation mapping process.

3.5.2 Uncertainty in Mapping L/S/IVOC Emissions

For L/S/IVOCs, the 2D-VBS framework was applied to aggregate predicted products into a reduced set of 15 representative CRACMM mechanism species. These representative species span a wide range of saturation concentrations (Ci^*) from 10^{-2} to 10^{6} μg m^{-3} and O:C ratios (nO:nC) from 0.1 to 0.8. The original 2D-VBS inventory is structured along a two-dimensional grid defined by $\log_{10}(Ci^*)$ and O:C ratio. During the mapping process to CRACMM, if a species in the 2D-VBS inventory could not be directly assigned to a CRACMM species, it was reassigned to the most proximate species in $\log_{10}(Ci^*)$ and/or O:C ratio. This reassignment process, while necessary, inevitably introduces additional uncertainty. The L/S/IVOC emission inventory used in this study is based on the work of Chang et al (Chang et al., 2022). For uncertainties associated with this inventory, readers are referred to the analysis by Chang et al., which discusses uncertainties related to emission factors, species classification, and spatial distribution.

4. Conclusions

https://doi.org/10.5194/egusphere-2025-3627
Preprint. Discussion started: 1 October 2025

This study introduces the newly mapped VOC and POA inventories (both traditional and full volatile) for CRACMM and presents the first comprehensive evaluation of $PM_{2.5}$ predictions using the newly developed CRACMM chemical mechanism. The performance of CRACMM with CB6r3_ae7, and Saprc07tic_ae7i are compared, and results demonstrate that CMAQ with CRACMM provides reliable predictions of $PM_{2.5}$ and its components across China during the months of January, April, July, and October 2021, although there are discrepancies in some complex regions.

In conclusion, the comparison of the three chemical mechanisms using the traditional POA inventory reveals that differences in R and MB values are generally small. However, with the replacement of the full volatile inventory, CRACMM tends to predict lower $PM_{2.5}$ concentrations in January across most regions of China except PRD and YRD. In the other months, CRACMM predicts higher concentrations than CB6r3_ae7 and Saprc07tic_ae7i when the full volatile inventory is incorporated. The differences in $PM_{2.5}$ concentrations in January, are primarily attributed to lower POA concentrations, which are influenced by semi-volatile partitioning and reduced aging of semi-volatile POA species under lower temperatures. In contrast, CRACMM simulates elevated SOA concentrations in eastern China due to enhanced precursor availability, while reduced SOA formation is observed in the SCB, where winter conditions slow the oxidation of precursors. The inclusion of the full volatile inventory in CRACMM results in higher SOA concentrations in October, driven by increased precursor availability. Overall, CRACMM demonstrates improved performance in terms of R and MB, particularly in January and October for the PRD region, but performs less well in April and July, particularly in the BTH region, compared to CB6r3_ae7. Additionally, CRACMM with the full volatile inventory increase in simulated $PM_{2.5}$ concentrations, resulting in smaller deviations from observation across many regions, highlighting the importance of including S/IVOC emissions in the chemical mechanism. Emission perturbation simulations using CMAQ further emphasize the significant role of various emission species, particularly BTX and SVOC, in driving $PM_{2.5}$ formation. The SOA contribution from BTX emissions accounts for nearly 50% of the $PM_{2.5}$ changes, while S/IVOC emissions primarily influence $PM_{2.5}$ through SOA formation. BTX emissions had a more significant impact in CB6r3_ae7, particularly in central China, partly due to the fewer VOC species included in the lumped BTX

https://doi.org/10.5194/egusphere-2025-3627
Preprint. Discussion started: 1 October 2025

of the CRACMM mechanism. Future assessments of O_3 predictions with CRACMM will offer additional constraints on the gas and aerosol chemistry that contributes to $PM_{2.5}$ formation.

Data availability. The model simulation is based on the CMAQ v5.4 developed by the U.S. EPA, and the code is publicly available at https://doi.org/10.5281/zenodo.7218076. All input data to reproduce the results and figures in this paper, has been archived on Zenodo (https://doi.org/10.5281/zenodo.16791307. Su et al., 2025) and is freely accessible.

Supplement. The supplement related to this article is available online at

Author contributions. LL and YJW designed the study. QFS conducted the modeling work, formal analysis and drafted the original manuscript. YFC contributed to data curation and emissions preparation. DCW contributed to model revision, manuscript editing and reviewing. HOTP, GS, BM, BP and YJW provided critical review and editing of the manuscript. LH and YJW contributed to modelling setup. LL supervised the project and secured funding.

Competing interests. The authors declare no conflicts of interest.

Disclaimer: The views expressed in this article are those of the authors and do not necessarily represent the views or the policies of the U.S. Environmental Protection Agency (EPA).

Acknowledgements. This study is financially supported by the National Key R&D Program of China (2025ZD1202005, 2025ZD1202001, 2025ZD1202004), the National Natural Science Foundation of China (nos. 42375102) and Shanghai International Science and Technology Cooperation Fund (24230740200). This work is supported by the Shanghai Technical Service Center of Science and Engineering Computing, Shanghai University.

References

Carlton, A. G., Bhave, P. V., Napelenok, S. L., Edney, E. O., Sarwar, G., Pinder, R. W., Pouliot, G. A., and Houyoux, M.: Model Representation of Secondary Organic Aerosol in CMAQv4.7, Environ. Sci. Technol., 44, 8553-8560,doi: 10.1021/es100636q, 2010.

Carter, W.: Implementation Of The Saprc-99 Chemical Mechanism Into The Models-3 Framework, 2000.

Carter, W. P. L.: DOCUMENTATION OF THE SAPRC-99 CHEMICAL MECHANISM FOR VOC REACTIVITY ASSESSMENT VOLUME 1 OF 2 DOCUMENTATION TEXT,

Carter, W. P. L.: Development of the SAPRC-07 chemical mechanism, Atmos. Environ., 44, 5324-5335,doi: 10.1016/j.atmosenv.2010.01.026, 2010.

Chang, X., Zhao, B., Zheng, H., Wang, S., Cai, S., Guo, F., Gui, P., Huang, G., Wu, D., Han, L., Xing, J., Man, H., Hu, R., Liang, C., Xu, Q., Qiu, X., Ding, D., Liu, K., Han, R., Robinson, A. L., and Donahue, N. M.: Full-volatility emission framework corrects missing and underestimated secondary organic aerosol sources, One Earth, 5, 403-412,doi: 10.1016/j.oneear.2022.03.015, 2022.

Chuang, K.-J., Yan, Y.-H., Chiu, S.-Y., and Cheng, T.-J.: Long-term air pollution exposure and

https://doi.org/10.5194/egusphere-2025-3627
Preprint. Discussion started: 1 October 2025

risk factors for cardiovascular diseases among the elderly in Taiwan, Occup. Environ. Med., 68, 64,doi: 10.1136/oem.2009.052704, 2011.

Derwent, R.: Intercomparison of chemical mechanisms for air quality policy formulation and assessment under North American conditions, J. Air Waste Manag. Assoc., 67, 789-796,doi: 10.1080/10962247.2017.1292969, 2017.

Goliff, W. S., Stockwell, W. R., and Lawson, C. V.: The regional atmospheric chemistry mechanism, version 2, Atmos. Environ., 68, 174-185,doi: 10.1016/j.atmosenv.2012.11.038, 2013.

Guenther, A. B., Jiang, X., Heald, C. L., Sakulyanontvittaya, T., Duhl, T., Emmons, L. K., and Wang, X.: The Model of Emissions of Gases and Aerosols from Nature version 2.1 (MEGAN2.1): an extended and updated framework for modeling biogenic emissions, Geosci. Model Dev., 5, 1471-1492,doi: 10.5194/gmd-5-1471-2012, 2012.

Huang, L., Wang, Q., Wang, Y., Emery, C., Zhu, A., Zhu, Y., Yin, S., Yarwood, G., Zhang, K., and Li, L.: Simulation of secondary organic aerosol over the Yangtze River Delta region: The impacts from the emissions of intermediate volatility organic compounds and the SOA modeling framework, Atmospheric Environment, 246, 118079,doi: 10.1016/j.atmosenv.2020.118079, 2021a.

Huang, L., Zhu, Y., Zhai, H., Xue, S., Zhu, T., Shao, Y., Liu, Z., Emery, C., Yarwood, G., Wang, Y., Fu, J., Zhang, K., and Li, L.: Recommendations on benchmarks for numerical air quality model applications in China – Part 1: PM2.5 and chemical species, Atmos. Chem. Phys., 21, 2725-2743,doi: 10.5194/acp-21-2725-2021, 2021b.

Kang, M., Hu, J., Zhang, H., and Ying, Q.: Evaluation of a highly condensed SAPRC chemical mechanism and two emission inventories for ozone source apportionment and emission control strategy assessments in China, Sci. Total Environ., 813, 151922,doi: 10.1016/j.scitotenv.2021.151922, 2022.

Kim, K.-H., Kabir, E., and Kabir, S.: A review on the human health impact of airborne particulate matter, Environ. Int., 74, 136-143,doi: 10.1016/j.envint.2014.10.005, 2015.

Koo, B., Knipping, E., and Yarwood, G.: 1.5-Dimensional volatility basis set approach for modeling organic aerosol in CAMx and CMAQ, Atmos. Environ., 95, 158-164,doi: 10.1016/j.atmosenv.2014.06.031, 2014.

Liu, J., Niu, X., Zhang, L., Yang, X., Zhao, P., and He, C.: Exposure risk assessment and synergistic control pathway construction for O3–PM2.5 compound pollution in China, Atmos. Environ. X., 21, 100240,doi: 10.1016/j.aeaoa.2024.100240, 2024.

Luecken, D. J., Yarwood, G., and Hutzell, W. T.: Multipollutant modeling of ozone, reactive nitrogen and HAPs across the continental US with CMAQ-CB6, Atmos. Environ., 201, 62-72,doi: 10.1016/j.atmosenv.2018.11.060, 2019.

Murphy, B. N., Woody, M. C., Jimenez, J. L., Carlton, A. M. G., Hayes, P. L., Liu, S., Ng, N. L., Russell, L. M., Setyan, A., Xu, L., Young, J., Zaveri, R. A., Zhang, Q., and Pye, H. O. T.: Semivolatile POA and parameterized total combustion SOA in CMAQv5.2: impacts on source strength and partitioning, Atmos. Chem. Phys., 17, 11107-11133,doi: 10.5194/acp-17-11107-2017, 2017.

Murray, C. J. L., Aravkin, A. Y., and Zheng, P.: Global burden of 87 risk factors in 204 countries and territories, 1990–2019: a systematic analysis for the Global Burden of Disease Study 2019, The Lancet, 396, 1223-1249,doi: 10.1016/S0140-6736(20)30752-

https://doi.org/10.5194/egusphere-2025-3627
Preprint. Discussion started: 1 October 2025

2, 2020.

Place, B. K., Hutzell, W. T., Appel, K. W., Farrell, S., Valin, L., Murphy, B. N., Seltzer, K. M., Sarwar, G., Allen, C., Piletic, I. R., D'Ambro, E. L., Saunders, E., Simon, H., Torres-Vasquez, A., Pleim, J., Schwantes, R. H., Coggon, M. M., Xu, L., Stockwell, W. R., and Pye, H. O. T.: Sensitivity of northeastern US surface ozone predictions to the representation of atmospheric chemistry in the Community Regional Atmospheric Chemistry Multiphase Mechanism (CRACMMv1.0), Atmos. Chem. Phys., 23, 9173-9190,doi: 10.5194/acp-23-9173-2023, 2023.

Pye, H. O. T. and Pouliot, G. A.: Modeling the Role of Alkanes, Polycyclic Aromatic Hydrocarbons, and Their Oligomers in Secondary Organic Aerosol Formation, Environ. Sci. Technol., 46, 6041-6047,doi: 10.1021/es300409w, 2012.

Pye, H. O. T., Luecken, D. J., Xu, L., Boyd, C. M., Ng, N. L., Baker, K. R., Ayres, B. R., Bash, J. O., Baumann, K., Carter, W. P. L., Edgerton, E., Fry, J. L., Hutzell, W. T., Schwede, D. B., and Shepson, P. B.: Modeling the Current and Future Roles of Particulate Organic Nitrates in the Southeastern United States, Environ. Sci. Technol., 49, 14195-14203,doi: 10.1021/acs.est.5b03738, 2015.

Pye, H. O. T., Pinder, R. W., Piletic, I. R., Xie, Y., Capps, S. L., Lin, Y.-H., Surratt, J. D., Zhang, Z., Gold, A., Luecken, D. J., Hutzell, W. T., Jaoui, M., Offenberg, J. H., Kleindienst, T. E., Lewandowski, M., and Edney, E. O.: Epoxide Pathways Improve Model Predictions of Isoprene Markers and Reveal Key Role of Acidity in Aerosol Formation, Environ. Sci. Technol., 47, 11056-11064,doi: 10.1021/es402106h, 2013.

Pye, H. O. T., Murphy, B. N., Xu, L., Ng, N. L., Carlton, A. G., Guo, H., Weber, R., Vasilakos, P., Appel, K. W., Budisulistiorini, S. H., Surratt, J. D., Nenes, A., Hu, W., Jimenez, J. L., Isaacman-VanWertz, G., Misztal, P. K., and Goldstein, A. H.: On the implications of aerosol liquid water and phase separation for organic aerosol mass, Atmos. Chem. Phys., 17, 343-369,doi: 10.5194/acp-17-343-2017, 2017.

Pye, H. O. T., Place, B. K., Murphy, B. N., Seltzer, K. M., D'Ambro, E. L., Allen, C., Piletic, I. R., Farrell, S., Schwantes, R. H., Coggon, M. M., Saunders, E., Xu, L., Sarwar, G., Hutzell, W. T., Foley, K. M., Pouliot, G., Bash, J., and Stockwell, W. R.: Linking gas, particulate, and toxic endpoints to air emissions in the Community Regional Atmospheric Chemistry Multiphase Mechanism (CRACMM), Atmos. Chem. Phys., 23, 5043-5099,doi: 10.5194/acp-23-5043-2023, 2023.

Robinson, A. L., Donahue, N. M., Shrivastava, M. K., Weitkamp, E. A., Sage, A. M., Grieshop, A. P., Lane, T. E., Pierce, J. R., and Pandis, S. N.: Rethinking Organic Aerosols: Semivolatile Emissions and Photochemical Aging, Science, 315, 1259-1262,doi: 10.1126/science.1133061, 2007.

Su, Q., Chen, Y: Datasets for 'Application and Evaluation of CRACMM Mechanism in $PM_{2.5}$ Simulation Over China' Zenodo [data set], https://doi.org/10.5281/zenodo.16791307, 2025.

Wang, Y., Ning, M., Su, Q., Wang, L., Jiang, S., Feng, Y., Wu, W., Tang, Q., Hou, S., Bian, J., Huang, L., Lu, G., Manomaiphiboon, K., Kaynak, B., Zhang, K., Chen, H., and Li, L.: Designing regional joint prevention and control schemes of PM2.5 based on source apportionment of chemical transport model: A case study of a heavy pollution episode, J. Clean. Prod., 455, 142313,doi: 10.1016/j.jclepro.2024.142313, 2024.

https://doi.org/10.5194/egusphere-2025-3627
Preprint. Discussion started: 1 October 2025

Woody, M. C., Baker, K. R., Hayes, P. L., Jimenez, J. L., Koo, B., and Pye, H. O. T.: Understanding sources of organic aerosol during CalNex-2010 using the CMAQ-VBS, Atmos. Chem. Phys., 16, 4081-4100,doi: 10.5194/acp-16-4081-2016, 2016.

Xie, Y., Paulot, F., Carter, W. P. L., Nolte, C. G., Luecken, D. J., Hutzell, W. T., Wennberg, P. O., Cohen, R. C., and Pinder, R. W.: Understanding the impact of recent advances in isoprene photooxidation on simulations of regional air quality, Atmos. Chem. Phys., 13, 8439-8455,doi: 10.5194/acp-13-8439-2013, 2013.

Yarwood, G., Rao, S., Yocke, M., and Whitten, G.: Updates to the carbon bond chemical mechanism: CB05 final report to the US EPA, RT-0400675, 2005.

Yarwood, G., Jung, J., Whitten, G. Z., Heo, G., Mellberg, J., and Estes, M.: UPDATES TO THE CARBON BOND MECHANISM FOR VERSION 6 (CB6),

Zhang, J., He, X., Gao, Y., Zhu, S., Jing, S., Wang, H., Yu, J. Z., and Ying, Q.: Estimation of Aromatic Secondary Organic Aerosol Using a Molecular Tracer—A Chemical Transport Model Assessment, Environ. Sci. Technol.,doi: 10.1021/acs.est.1c03670, 2021.